Journal of Materials Chemistry C

Coil-rod-coil triblock copolymers synthesized by macromolecular clicking and their compatibilizer effects in all-polymer solar cells

Journal:	*Journal of Materials Chemistry C*
Manuscript ID	TC-ART-10-2021-004948.R1
Article Type:	Paper
Date Submitted by the Author:	13-Nov-2021
Complete List of Authors:	Otep, Sultan; Tokyo Institute of Technology Tseng, Yu-Cheng; National Taiwan University Yomogita, Naomasa; Tokyo Institute of Technology Chang, Jia-Fu; National Taiwan University Chueh, Chu-Chen; University of Washington, Department of Materials Science and Engineering Michinobu, Tsuyoshi; Tokyo Institute of Technology, Department of Materials Science and Engineering

Coil-rod-coil triblock copolymers synthesized by macromolecular clicking and their compatibilizer effects in all-polymer solar cells†

Sultan Otep,[a] Yu-Cheng Tseng,[b] Naomasa Yomogita,[a] Jia-Fu Chang,[b] Chu-Chen Chueh[b,*] and Tsuyoshi Michinobu[a,*]

[a] *Department of Materials Science and Engineering, Tokyo Institute of Technology, 2-12-1 Ookayama, Meguro-ku, Tokyo 152-8552, Japan. E-mail: michinobu.t.aa@m.titech.ac.jp*

[b] *Department of Chemical Engineering and Advanced Research Center for Green Materials Science and Technology, National Taiwan University, Taipei 10617, Taiwan. E-mail: cchueh@ntu.edu.tw*

† Electronic supplementary information (ESI) available. See DOI:

Abstract

Poly(diethynylthiophene) (**PDET**) synthesized via Hay coupling polycondensation retains terminal alkynes for tethering polystyrene (PS) blocks by a simple Cu-catalyzed azide-alkyne click (CuAAC) reaction. Successful syntheses of triblock copolymers were confirmed by ^{1}H NMR, FTIR, and GPC measurements. Optical and electrochemical properties of the **PDET** block were conserved in the triblock copolymers, as determined from the UV-vis absorption spectra and redox potentials. Surface topography of the polymer films revealed the micrometer-scale features attributable to phase separation, which was supported by thermal analyses. The compatibilizer functions of **PDET** and triblock copolymer **P1** were investigated and compared in all-polymer solar cells (all-PSCs). Addition of 1 wt% **P1** was shown to result in an enhanced power conversion efficiency (PCE) from 5.90% to 6.24%, corresponding to a relative increase of ~6%, whereas adding 1 wt% **PDET** decreased the resultant PCE. Notably, adding a proper compatibilizer helped reduce device's potential loss, as evidenced by the improved V_{oc} for the 1 wt% **P1** device. Our results highlight the critical role of the coil segment in designing block copolymer-based compatibilizers for all-PSCs. Also, this study demonstrates a straightforward synthetic route for the coil-rod-coil triblock copolymers that afford a compatibilizer function suitable for all-PSCs.

Introduction

Block copolymers have been conventionally synthesized by sequentially adding different monomers in living polymerization systems.[1,2] In another approach, macromolecular coupling of pre-made reactive polymers by highly efficient click chemistry reactions, such as Cu-catalyzed azide-alkyne cycloaddition (CuAAC), is recently often adopted to produce various diblock copolymers[3–8] and multiblock copolymers.[9–12] Of these, rod-coil block copolymers are mostly based on poly(3-hexylthiophene) (P3HT) tethered to non-conjugated polymers, such as polystyrene and polyvinylpyrrolidone. This is because terminal alkyne-substituted P3HT can be prepared by Grignard metathesis polymerization and it is a suitable platform for macromolecular CuAAC coupling with azide-substituted counter polymers. On the other hand, rigid polymer backbones with terminal alkynes at both sides are required to synthesize coil-rod-coil block copolymers by a similar CuAAC coupling approach. In addition, to expand the scope of the macromolecular coupling approach, rigid conjugated polymer backbones other than P3HT are desired. In this context, we noted that poly(arylenebutadiynylene)s are readily prepared by self-polycondensation of diethynylarylene monomers and can possess two terminal alkynes if no side reactions occur during polymerization. In addition, various aromatic monomers can be designed, which enables us to expand a library of coil-rod-coil block copolymers. Furthermore, poly(arylenebutadiynylene)s were recently shown to be an effective crosslinking matrix and their charge-transport and light-harvesting properties can be tuned by the degree of crosslinking.[13,14] However, no block copolymers of poly(arylenebutadiynylene)s have, to the best of our knowledge, been reported so far.

In recent years, bulk heterojunction (BHJ) design has become the most prevailing and efficient system for organic photovoltaics (OPVs), which consists of an interpenetrating network formed by an electron-rich (donor) conjugated molecule and an electron-deficient (acceptor) conjugated molecule. At an earlier time, acceptors were generally made from fullerene derivatives and they have realized power conversion efficiencies (PCEs) approaching 12%.[15–17] However, limited

by their weak light absorption, the development of fullerene–based OPVs has encountered a bottleneck. To this end, the exploitation of non-fullerene small molecules received increasing research attention and has significantly pushed the PCE to over 17% in single junction OPVs.[18–20] The rapid rise of non-fullerene small molecules also encouraged the development of n-type conjugated polymers for realizing efficient all-polymer solar cells (all-PSCs), and the state-of-the-art PCEs have just recently exceeded 10%.[21–34]

Besides the significant efforts in developing new polymer donors and acceptors, another promising approach for optimizing PCEs is to construct a ternary BHJ blend incorporating a third component that is called "compatibilizer" or "additive".[35-37] For example, Hou *et al.* reported a noticeably enhanced PCE (from 5.53 to 7.07%) for the PCE12:N2200-based all-PSC by adding a high boiling point solvent of 1,8-diiodooctane (DIO).[38] Additives of π-conjugated small molecules and polymers were also reported to possess similar effects for all-PSCs.[39] For example, Chen *et al.* introduced a BDT-based conjugated polymer (J71) as a compatibilizer to improve the PCE of the all-PSC comprising PCE12 and NDI-based acceptor polymer (PNDI-2T-TR(5)) from 7.51 to 9.05%.[40]

We recently demonstrated the effective compatibilizer function for a series of rod-coil or coil-rod-coil block copolymers that were synthesized by the nucleophilic substitution reaction of the propagation anion of polystyrene to the bromoalkane terminals of P3HT.[41–43] When the block copolymers were employed as P3HT:PCBM interfacial compatibilizers, it was found that the coil-rod-coil triblock copolymer has a superior compatibilizer effect to the coil-rod diblock copolymer due to the higher crystallization capability of the P3HT domain. In addition, the triblock copolymer had a higher thermal property than the diblock copolymer. Many other block copolymer-based compatibilizers were also reported by scientists in the field.[44,45] However, it should be noted that the syntheses of all these block copolymers require multi-step reactions involving strict living polymerization techniques. In addition, most of these block copolymer compatibilizers were employed for fullerene- and non-fullerene small molecule acceptor-based OPVs.[46–50] To the best of

our knowledge, no coil-rod-coil block copolymers have been applied as the interfacial compatibilizers for all-PSCs thus far, although an all-conjugated block copolymer was recently found to become an effective compatibilizer.[51]

Based on the above consideration,[41–43] in this study, we selected poly(diethynylthiophene) (**PDET**) as the "rod" platform and it was successfully reacted with two equivalents of azide-substituted "coil" polystyrene under CuAAC conditions to yield a series of coil-rod-coil block copolymers, **PS$_m$-*b*-PDET$_n$-*b*-PS$_m$**. Both **PDET** and **PS$_{37}$-*b*-PDET$_{29}$-*b*-PS$_{37}$** (**P1** as a representative) were investigated as the compatibilizers for an all-PSC based on the PCE12:N2200 blend. It was shown that adding 1 wt% **P1** into the binary blend can deliver a relative ~6% enhancement in PCE; whereas, adding 1 wt% **PDET** did not provide any positive effects on the photovoltaic performance. This result clearly suggests that the coil-rod-coil triblock copolymer design provides a more prominent compatibilizer function. Besides, we also unveiled that the compatibilizer can help reduce device's potential loss to produce a higher open-circuit voltage than the control device as benefitted from its capability of tuning the BHJ morphology of the blend film.

Results and Discussion

Synthesis of block polymers

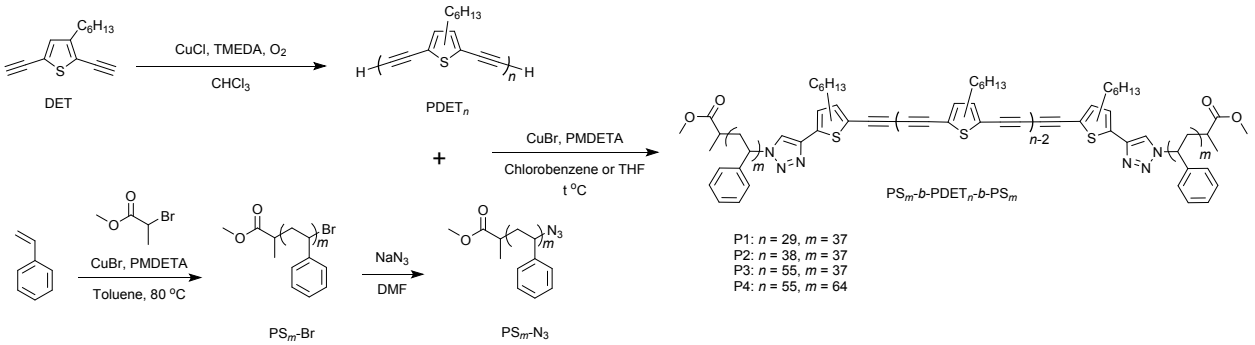

Scheme 1. Synthetic routes for **PS$_m$-*b*-PDET$_n$-*b*-PS$_m$** triblock copolymers, **P1**, **P2**, **P3** and **P4**.

We recently reported the synthesis of poly(3-hethylthiophene-2,5-diylbutadiynylene)

(**PDET**) by self-polycondensation of 2,5-diethynyl-3-hexylthiophene (DET) using Hay coupling with CuCl/*N*,*N*,*N*',*N*'-tetramethylethylenediamine (TMEDA) catalysts in the presence of air at room temperature (Scheme 1).[52] Due to the limited chemical stability of DET in air, the monomer was placed into a polymerization flask in the form of a *n*-hexane solution (174 mg in 1 mL). However, in this work, we improved the polymerization rate by increasing the monomer concentration (154 mg in 0.3 mL), which also resulted in higher number-average molecular weights (M_ns). This allowed us to control the molecular weights of **PDET**. Polymerizations were quenched after 40 and 60 min to synthesize two **PEDTs** with the M_n values (estimated from GPC) of 8.14 kg mol^{-1} (named as **PDET$_{38}$**) and of 11.8 kg mol^{-1} (named as **PDET$_{55}$**), respectively (Table S1, ESI†). Although it was possible to synthesize **PDET** with a M_n value of up to 20 kg mol^{-1} by this method, it was decided to limit its M_n value in the range of ~10 kg mol^{-1} to better match those of the PS parts of the targeted triblock copolymers (vide infra). The presence of terminal alkynes in **PDET** was confirmed from the ^{1}H NMR peak at 3.49 ppm and FTIR signal at 3309 cm^{-1} (≡C−H stretching). The M_n values of the polymers were estimated by comparing the ^{1}H NMR peak areas of the terminal alkynes to those of the repeat DET units (Figure S1 and S2, ESI†), showing a good agreement with the values determined by GPC (Table S1, ESI†). This also demonstrated that there are no noticeable side reactions at the terminal alkynes during polymerization. Therefore, **PDET$_{38}$** and **PDET$_{55}$** together with the previously reported **PDET** (labeled as **PDET$_{29}$**)[52] were employed for the synthesis of triblock copolymers, because the alkynes of polymer terminals are a functional group suitable for click chemistry-based post-modification reactions.

Lutz and Matyjaszewski have showed that the synthesis of Br-functionalized polystyrene (PS-Br) is a trade-off between conversion (linked to M_n) and functionality of the terminal Br, thus leading to the optimized M_n values of PS-Br to less than ~10 kg mol^{-1}.[53] They also found that high M_n value and high end-group functionality can be achieved simultaneously by using high monomer-

to-catalyst/initiator ratio and quenching the polymerization at early stages. According to this method, PS_{37}-Br with a M_n value of 3.97 kg mol^{-1} and PS_{64}-Br with a M_n value of 6.85 kg mol^{-1} (estimated from GPC) were synthesized (Table S1, ESI†). The polydispersity ($Đ$: M_w/M_n) was 1.05 for both polymers. Their degree of polymerization (DP), estimated from the ^{1}H NMR spectroscopy (Figure S3 and S4, ESI†), showed a good agreement with the GPC results and the difference was merely two repeat units. The integration ratio of the ^{1}H NMR signal corresponding to −CH−Br (4.35–4.59 ppm) against the one associated with the terminal $-OCH_3$ (3.37–3.54 ppm) suggested that the Br-functionalization was over 90% for both polymers. An azido-functionalized polystyrene (PS-N_3) was then synthesized by reacting the corresponding PS-Br with an excess sodium azide (NaN_3), following the procedure reported in literature.[54] Successful formation of PS_{37}-N_3 and PS_{64}-N_3 was confirmed by ^{1}H NMR and FTIR spectroscopies. In the ^{1}H NMR spectra, the signal at 4.35–4.59 ppm (−CH−Br) disappeared, while a new broad peak at 3.90 ppm ($-CH-N_3$) appeared (Figure S5, ESI†). The integration ratio of the signals confirmed that the azido-functionality (f_{N3}) of the polymers is in line with those of the corresponding PS-Br polymers. In addition, a strong signal at 2097 cm^{-1}, ascribed to the N=N=N stretching, appeared in the FTIR spectra (Figure S6–9, ESI†). GPC results suggested that the $Đ$ values of the obtained PS-N_3 polymers were the same as the starting PS-Br polymers.

Triblock copolymers, **PS$_m$-*b*-PDET$_n$-*b*-PS$_m$**, were then synthesized by the CuAAC click reaction between **PDET** and a slight excess of PS-N_3 using CuBr/*N*,*N*,*N*',*N*'',*N*''-pentamethyldiethylenetriamine (PMDETA) as the catalysts.[54] The reaction was conducted either in chlorobenzene or tetrahydrofuran (THF). After the reaction, the crude product mixture was thoroughly washed with acetone to remove the unreacted PS-N_3. The targeted triblock copolymers were extracted with cold chloroform, leaving behind insoluble solids, which could be the products of further polycondensation and/or cross-linking of **PDET**.[52] Thus, four triblock copolymers **P1** (**PS$_{37}$-**

***b*-PDET$_{29}$-*b*-PS$_{37}$**), **P2** (**PS$_{37}$-*b*-PDET$_{38}$-*b*-PS$_{37}$**), **P3** (**PS$_{37}$-*b*-PDET$_{55}$-*b*-PS$_{37}$**), and **P4** (**PS$_{64}$-*b*-PDET$_{55}$-*b*-PS$_{64}$**) were obtained in 43–53% yields. The ^{1}H NMR peaks at 3.90 ppm ascribed to CH−N$_3$ of PS-N$_3$ and 3.49 ppm ascribed to ≡CH of **PDET** disappeared, while the other characteristic signals were present, confirming the successful macromolecular clicking (see Figure 1a for **P1**). In addition, FT-IR signals at 2097 cm^{-1} (N=N=N stretching) and 3309 cm^{-1} (≡C−H stretching) disappeared, which indicated that all the terminal alkynes of **PDET** and azide groups of PS-N$_3$ were used up (Figure 1b and Figure S8–S10, ESI†). GPC measurements revealed that the M_n values of triblock copolymers were close to those expected from the reacted PS-N$_3$ and **PDET** polymers (Table 1). Notably, the $Đ$ values for the triblock copolymers decreased compared to those of the starting **PDET** polymers (Figure 1c and Figure S11, ESI†). In addition, a comparison of the ^{1}H NMR peak integration value at 3.37–3.54 ppm (−OCH$_3$) to those of the repeat DET units allowed to estimate the extent of the click reaction. For example, the ^{1}H NMR of **P1** suggested that there were 31 repeat DET units per PS chain. This result indicated that 7% of the **PDET$_{29}$** chains were not clicked to PS, probably caused by the loss of terminal alkynes under the click reaction conditions. However, due to the unlikelihood of losing both terminal alkynes on a single polymer chain, it is assumed that at most 14% of **PDET$_{29}$** formed the diblock copolymer with PS$_{37}$. The incomplete click reactions led to the observed lower M_n value in GPC than the expected values (see **P1**, **P3** and **P4** in Table 1).

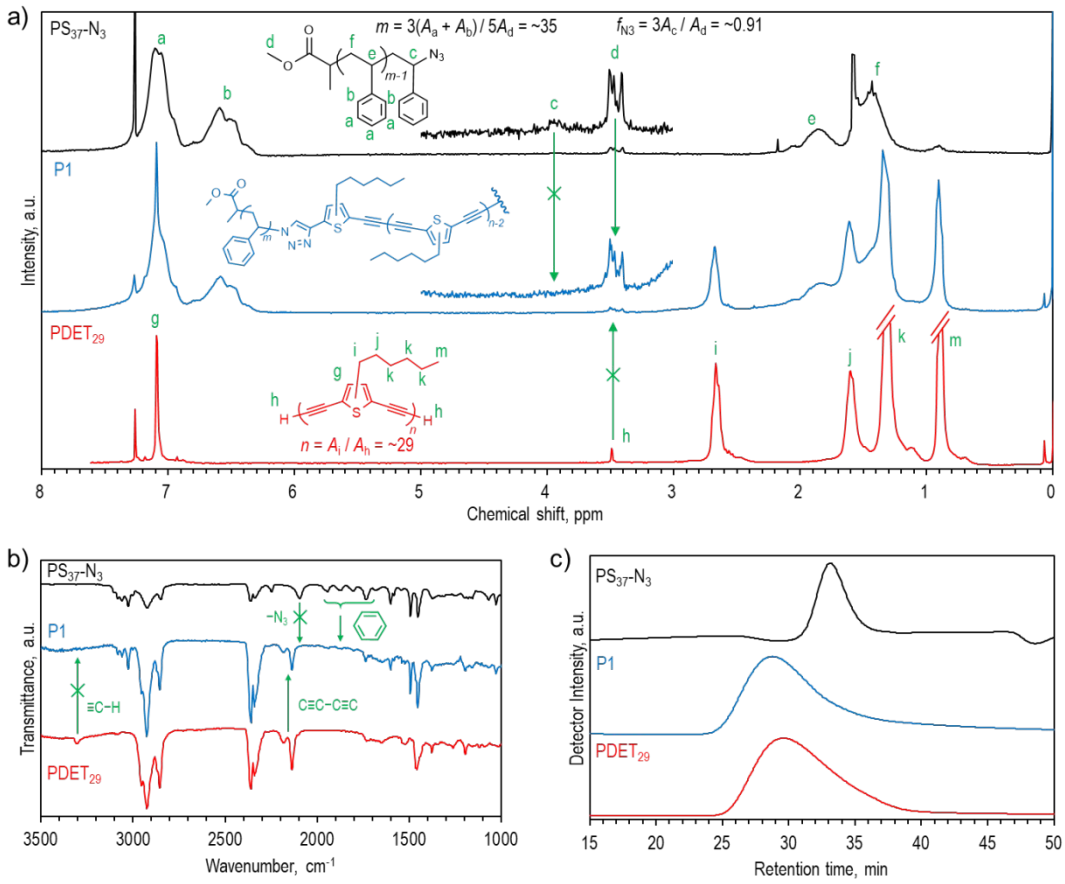

Figure 1. Evidence of successful synthesis of **P1** by comparing a) ^{1}H NMR spectra, b) FTIR spectra, and c) GPC curves of PS_{37}-N_3, **PDET$_{29}$**, and **P1**. Magnified regions of the ^{1}H NMR spectra at 3–5 ppm are provided for PS_{37}-N_3 and **P1** to visualize the peak associated with $-N_3$. All the ^{1}H NMR and FTIR spectra as well as the GPC curves were normalized and manually offset for the convenience of visualization. For **P2**, **P3** and **P4**, see Supporting Information (Figure S8–S11, ESI†).

Table 1. Summary of click reactions between **PDET** and PS-N_3.

Polymer	**Measured M_n [a] (kg mol^{-1})**	**Đ**	**Expected M_n [b] (kg mol^{-1})**	**Click reaction conditions [c]**
P1 (n = 29, m = 37)	13.6	2.04	14.1	chlorobenzene, 4 h, 80 °C
P2 (n = 38, m = 37)	16.2	2.56	16.0	THF, 7 h, 60 °C
P3	18.9	2.34	19.6	THF, 4 h, 60 °C

(n = 55, m = 37)				
P4 (n = 55, m = 64)	23.5	2.21	25.3	THF, 4 h, 60 °C

[a)] Measured in GPC with *o*-dichlorobenzene at 40 °C and molecular weights estimated by comparing to polystyrene standards. [b)] Calculated from the M_ns of the starting **PDET** and PS-N_3, assuming 100% reaction yield. [c)] All reactions performed under Ar atmosphere using dry solvents and pre-purified CuBr catalyst.

Thermal properties

Thermogravimetric analysis (TGA) showed that **PDET$_{29}$** had the onset of weight loss (decomposition temperature, T_d) at 352 °C, while this value shifted to 261 °C for **P1**, which was closer to the T_d of PS_{37}-N_3 (Figure 2a and Table 2). In addition, the TGA curve of **P1** had two slopes corresponding to the decomposition of **PDET$_{29}$** and PS_{37}-N_3. The **PDET** content of **P1** estimated from the TGA curve was 59% by mass. This value is higher than those calculated from the ^{1}H NMR spectra (47%) and GPC (44%). Thus, the above result must be considered with care, since the decomposition rates of **PDET$_{29}$** and PS_{37} in **P1** might be different than those of the pristine polymers. For example, it was previously shown that **PDET** undergoes cross-linking by 1,4-addition of 1,3-butadiyne moieties at temperature (T) above 110 °C.[55] This can be clearly seen from the exothermic peaks ($T_{exo,1}$ and $T_{exo,2}$) in the differential scanning calorimetry (DSC) curve of **PDET$_{29}$** (Figure 2b). While the $T_{exo,1}$ disappeared in **P1**, $T_{exo,2}$ was present, indicating that **PDET$_{29}$** in **P1** still underwent cross-linking at >150 °C. The sample turned completely black after heating to 250 °C, which further supports the possibility of cross-linking.[55] As cross-linking was shown to negatively affect the semiconducting properties of **PDET**, the increase in the cross-linking initiation temperature should be beneficial for **P1**. PS_{37}-N_3 exhibited a glass transition temperature (T_g) at 89 °C, which was in agreement with the results reported earlier.[54] In addition, decomposition of the azide group ($T_{d,N3}$) was observed at 158 °C.[56] The PS_{37} in **P1** retained its T_g at nearly the same temperature. The

endothermic peaks of PS_{37}-N_3 and **P1** at ~50 °C disappeared in the 2nd heating scan (Figure S12, ESI†).

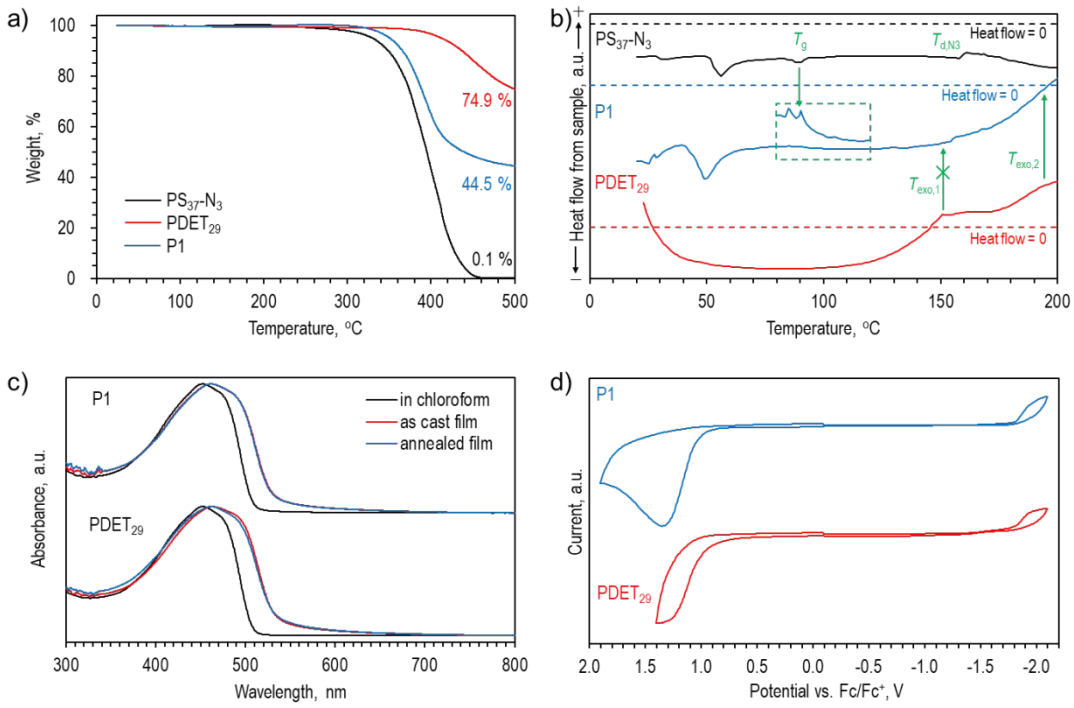

Figure 2. Comparison of a) TGA curves, b) DSC curves (1st heating scan), c) UV-vis absorption spectra and d) CV curves of **PDET$_{29}$** and **P1**. DSC curves, UV-vis spectra and CV curves were normalized and manually offset for the convenience of visualization.

Optical and electrochemical properties

PDET$_{29}$ and **P1** exhibited identical light absorption spectra with an optical bandgap ($E_{g,opt}$) of 2.34 eV (Figure 2c and Table 2). The absorption spectra of as-cast thin films showed a notable red-shift (~10 nm) as compared to the corresponding solution spectra, indicating substantial aggregation in the thin films. Cyclic voltammograms (CVs) of the thin films of **PDET$_{29}$** and **P1** exhibited irreversible oxidation and reduction steps. Both polymers displayed the highest occupied molecular orbital (HOMO) energy level (E_{HOMO}) of −5.8 eV and lowest unoccupied molecular orbital (LUMO)

energy level (E_{LUMO}) of −3.0 eV. Similar optical and electrochemical results were obtained for **P2**, **P3** and **P4** (Figure S13, ESI†). These results were somewhat expected, since attaching PS blocks did not alter the fundamental electronic properties of the **PDET** backbone. In addition to this, **PDET$_{38}$** and **PDET$_{55}$** had no difference in the UV-vis absorption spectra and CV curves compared to **PDET$_{29}$** (Figure S13, ESI†), suggesting that all **PDETs** reached the effective conjugation length.[57] The identical UV-vis absorption spectra also indicated that the molecular packing motif does not change among these polymers.[58]

Table 2. Summary of thermal, electrochemical and optical properties of PS_{37}-N_3, **PDET$_{29}$** and **P1**.

Polymer	T_d a) (°C)	T_g b) (°C)	T_{exo} c) (°C)	E_{HOMO} d) (eV)	E_{LUMO} d) (eV)	λ_{max}^{sol} e) (nm)	λ_{max}^{film} e) (nm)	λ_{onset} e) (nm)	$E_{g,opt}$ e) (eV)
PS_{37}-N_3	255	89	158	–	–	–			–
PDET$_{29}$	352	–	154, 206	−5.78	−3.05	452	463	531	2.34
P1	261	~90	>200	−5.81	−3.02	452	461	531	2.34

a) Determined from the onset of mass loss in TGA curve. b) Determined from step change in the heating cycle of DSC curve. c) Other exothermic peaks. d) Determined from the onsets of oxidation and reduction peaks in CV. e) UV-vis absorption maxima of $CHCl_3$ solution (λ_{max}^{sol}) and as-cast film (λ_{max}^{film}). Onset of UV-vis absorption band (λ_{onset}) of as-cast films. $E_{g,opt}$ calculated from λ_{onset} of as-cast films.

AFM measurements

Tapping-mode atomic force microscopy (AFM) topographical images of the as-cast films of **P1**, **P2**, **P3** and **P4** on an octadecyltrimethoxysilane-modified Si/SiO_2 substrate exhibited smooth surfaces (Figure 3). When the films were annealed at a temperature slightly above the T_g of the PS block (at 120 °C), distinct surface features appeared for each polymer. **P1** formed isolated spherical

particles with the diameters of up to 200 nm and height of up to 60 nm. In case of the **P2** film, these spheres were even larger with the cross section of up to 500 nm and height of up to 120 nm. Interestingly, the spheres were much smaller in the **P3** film (<100 nm in diameter), while new interconnected stripes were formed. The larger area scan image (Figure S14, ESI†) showed that this network covered the entire surface and an individual stripe spanned up to several micrometers uninterruptedly. In the **P4** film, more sphere-like particles were again observed. The spheres were interconnected as in the case of **P3**. Such changes in surface morphology suggested possible phase separation undergoing in these triblock copolymer films. Notably, different surface structures could be achieved by modifying the molecular weights of the polymer blocks.

Stripe-like morphology of the annealed **P3** film can be explained from the low PS content both in terms of mass fraction (42%) and chain length (29%). Shorter PS blocks would make it difficult self-assemble into spherical particles. In contrast, the mass fraction of the PS blocks in **P1**, **P2** and **P4** were in the range of 50–60%, and about 40% of the single polymer chain length was PS. It was thus possible to form larger spheres for **P1** and **P2**. In the case of **P4**, much longer PS chains could allow to entangle and form more interconnected spherical particles. A delicate balance between the coil and rod fraction in the triblock copolymers produced unique thermodynamically stable self-assembled structures.

For comparison, AFM images of as-cast and annealed $\mathbf{PDET_{29}}$ and **P1** films were also measured (Figure S15, ESI†). Both as-cast and annealed $\mathbf{PDET_{29}}$ films showed relatively smooth surfaces, expectedly indicating that there was no phase separation. Annealing of **P1** at a temperature closer to its T_g (100 °C) did not result in phase separation as well, suggesting that the temperature was not enough to mobilize the polymer chains. Interestingly, when the **P1** film was rapidly heated to 200 °C, the surface roughened but the structures were different from those previously observed in the films annealed at 120 °C. The underlying surface still resembled that of the **P1** film annealed at

100 °C. These findings allowed us to theorize that as the temperature quickly rose above T_g, the phase separation did not have enough time to occur. Instead, cross-links could form at >150 °C and stiffen the film fixing the initial surface morphology. It is worth noting that substrates are usually not heated to temperatures as high as 200 °C in the device fabrication process to avoid macro-phase separation.

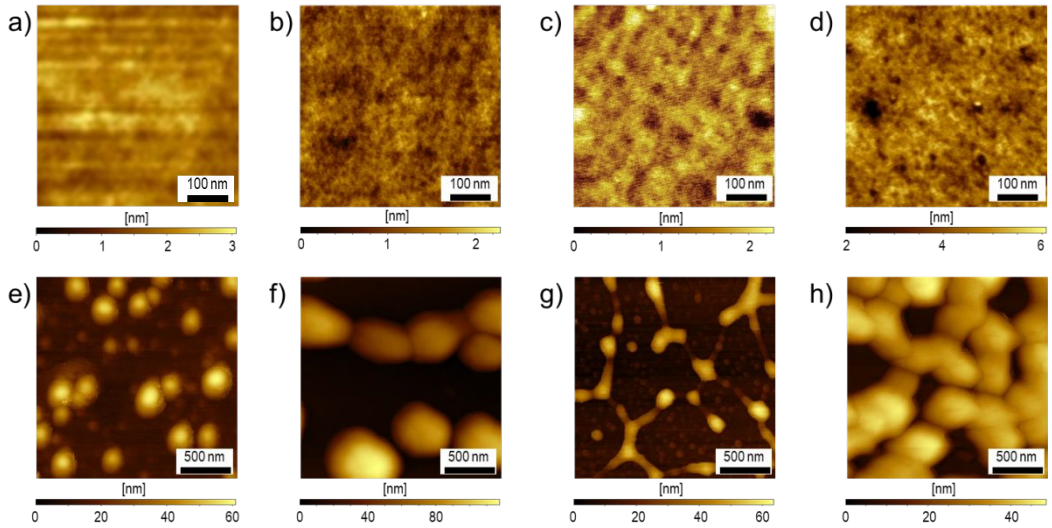

Figure 3. Tapping-mode AFM topographical images of the as-cast films of a) **P1** (magnified by a factor of 2 from the original image), b) **P2**, c) **P3** and d) **P4** and the annealed films of e) **P1**, f) **P2**, g) **P3** and h) **P4**. Films were annealed on a hotplate at 120 °C for 30 min.

Compatibilizer effect in all-PSCs

We have previously demonstrated the compatibilizer effect for a series of coil-rod-coil block copolymers in the fullerene- and non-fullerene small molecule-based OPVs.[41–43] We herein investigate the compatibilizer effect of the synthesized **PDET$_{29}$** (referred as **PDET** hereafter) and **P1** in an all-PSC using a representative PCE12:N2200 BHJ blend and compare their difference (Figure 4a). Details of device fabrication are described in the Experimental Section. Figure 4b shows current density-voltage (*J*-*V*) curves of the fabricated all-PSCs measured under AM 1.5G illumination, and the relevant photovoltaic parameters, including open-circuit voltage (V_{oc}), short-circuit current (J_{sc}),

fill factor (FF), and photoconversion efficiency (PCE), are summarized in Table 3.

As seen, the control device showed a decent maximum PCE (PCE_{max}) of 5.90% with a V_{oc} of 0.878 V, a J_{sc} of 11.50 mA/cm^2, and a FF of 58.44%. After adding the compatibilizers, the performance of the derived device showed a distinctly different change. Compared to the control device, the device added with 1 wt% **P1** showed an improved PCE_{max} of 6.24% with a slightly larger V_{oc} of 0.883 V, a similar J_{sc} of 11.50 mA/cm^2, and an increased FF of 61.45%. Considering the mismatched energy levels of **P1** to those of PCE12 and N2200, such a performance enhancement suggests the potential compatibilizer effect for **P1**. That is, adding **P1** enables a better BHJ morphology. In contrast, the device added with 1 wt% **PDET** gave a lousy PCE_{max} of 4.91% with a decreased V_{oc} of 0.862 V, a largely decreased J_{sc} of 9.64 mA/cm^2, and a similar FF of 59.05%. These results clearly unveil the important role of the block copolymer design on the resultant compatibilizer function. Similar to the previous results reported in literature,[43] the coil-rod-coil triblock **P1** demonstrated a more prominent compatibilizer function. This highlights the critical function of the coil segment in mediating the BHJ morphology and this will be discussed later. Despite a decent compatibilizer effect, the tolerance of **P1** in the BHJ blend was limited to below 1 wt%, mainly due to its insulating property and the phase aggregation induced by the excess amount of block copolymers. The device performance decreased to a PCE_{max} of 5.33% with a V_{oc} of 0.877 V, a J_{sc} of 10.04 mA / cm^2, and FF of 60.73 % as the blending amount of **P1** was increased to 3 wt%.

Figure 4c presents the external quantum efficiencies (EQE) of these devices. Compared to the control device, the device added with 1 wt% of **P1** slightly enhanced photoresponse in the wavelength region of 400-800 nm. Inset in Figure 4c shows the relative improvement of the EQE, which is clearly contributed from the enhanced absorption of PCE12 and N2200. On the other hand, both devices with 1 wt% **PDET** and 3 wt% **P1** exhibited much reduced photoresponse. This result suggests that the original BHJ morphology underwent undesired phase separation, resulting in a poor carrier collection. Notably, for the device with 3 wt% **P1**, an additional peak at 400-500 nm appeared

and it might have arisen from the absorption of **P1** (Figure 2c). Also, the changed EQE profile compared to that of the control device again suggests that the excess **P1** varied the phase aggregation of the BHJ blend.

Table 3. Photovoltaic performance of the fabricated all-PSCs.

	V_{OC} (V)	J_{SC} (mA / cm^2)	FF (%)	PCE$_{max}$ (%) [b)]
Control [a)]	0.878 (0.863 ± 0.015)	11.50 (11.30 ± 0.2)	58.44 (57.61 ± 0.83)	5.90 (5.61 ± 0.29)
1 wt% PDET	0.862 (0.843 ± 0.023)	9.64 (9.47 ± 0.51)	59.05 (58.17 ± 3.53)	4.91 (4.65 ± 0.32)
1 wt% P1	0.883 (0.875 ± 0.008)	11.50 (11.37 ± 0.13)	61.45 (59.70 ± 1.75)	6.24 (5.93 ± 0.31)
3 wt% P1	0.877 (0.832 ± 0.045)	10.04 (10.10 ± 0.58)	60.73 (57.64 ± 4.73)	5.33 (4.84 ± 0.57)

[a)] PCE12:N2200 BHJ system. [b)] The average PCEs shown in the table are based on 15 devices.

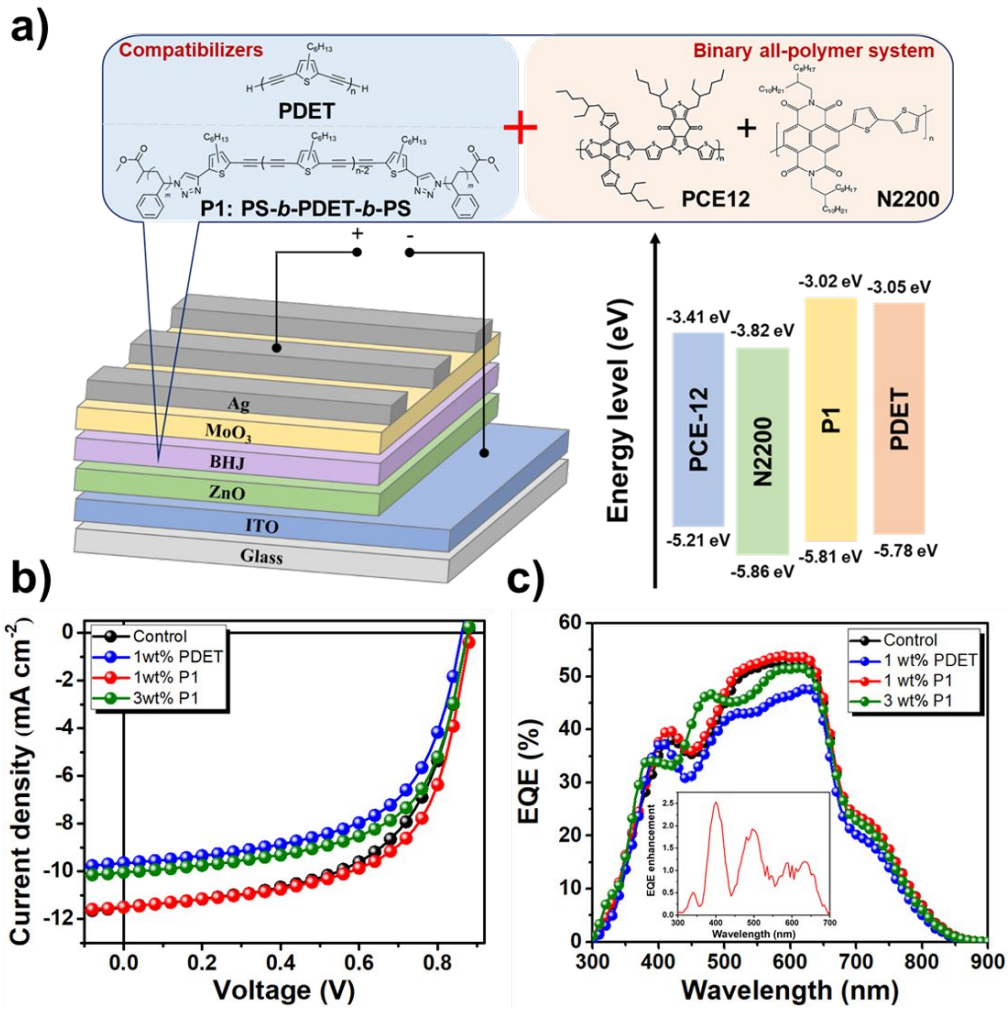

Figure 4. a) Schematic configuration and the energy-level diagram of the device and the chemical structures of the studied materials. (b) The *J-V* and (c) EQE curves of the fabricated all-PSCs using different compatibilizers. Inset in (c) shows the relative improvement in the EQE between the control device and 1 wt% **P1** device.

Charge recombination behaviors of these devices were investigated by plotting photocurrent density (J_{ph}) as a function of effective voltage (V_{eff}), as shown in Figure 5a. J_{ph} is defined by the equation of $J_{ph} = J_L - J_D$, where J_L and J_D stand for the current density under AM 1.5G illumination and in the dark condition, respectively, and V_{eff} is defined as $V_{eff} = V_0 - V_{bias}$, where V_0 is the voltage while J_{ph} is zero and V_{bias} is the applied bias. J_{ph} generally approaches a saturated value (J_{sat}) at the

high bias region, and under this condition, charges will fully dissociate into free carriers and sweep out by the electric field. Under the maximum power output condition, the charge collection probability can be evaluated by the ratio of $J_{ph,max}/J_{sat}$, and the exciton dissociation probability can be estimated by the ratio of $J_{ph,sc}/J_{sat}$ under the short-circuit condition. It thus can be expected that only parts of photogenerated excitons dissociate into free carriers and collected by electrodes at a certain V_{eff} between the short-circuit condition and maximum power output condition, and the charge dissociation and collection probabilities can be calculated by the ratio of J_{ph}/J_{sat}.[59] As seen, at the same V_{eff} of 0.1 V, the estimated probabilities for the control, 1 wt% **P1**, and 1wt% **PDET** all-PSCs were 0.54, 0.60, and 0.56, respectively. The highest value observed for the 1 wt% **P1** device suggests its most efficient charge dissociation and collection capability among the studied devices. Figure 5b displays the dependence of J_{sc} on various light intensities (P_{light}). The relationship between them follows a power-law dependence with respect to the equation of $J_{sc} \propto (P_{light})^{\alpha}$. Generally, α value approaching 1.0 indicates that all the dissociated free carriers are collected by electrodes before bimolecular recombination, while the α value smaller than 1.0 suggests the occurrence of bimolecular recombination.[60,61] As shown, all of the fabricated devices showed a linear dependence of J_{sc} on P_{light} with a logarithmic plot. Among them, the 1 wt% **P1** device possessed the highest α value of 0.9896, implying its extremely low bimolecular recombination. The above result clearly supports the performance enhancement observed for the 1 wt% **P1** device. Again, as considering the electronic properties and energy levels of **P1**, such enhancement should stem from the optimization of BHJ morphology of the photoactive blend.

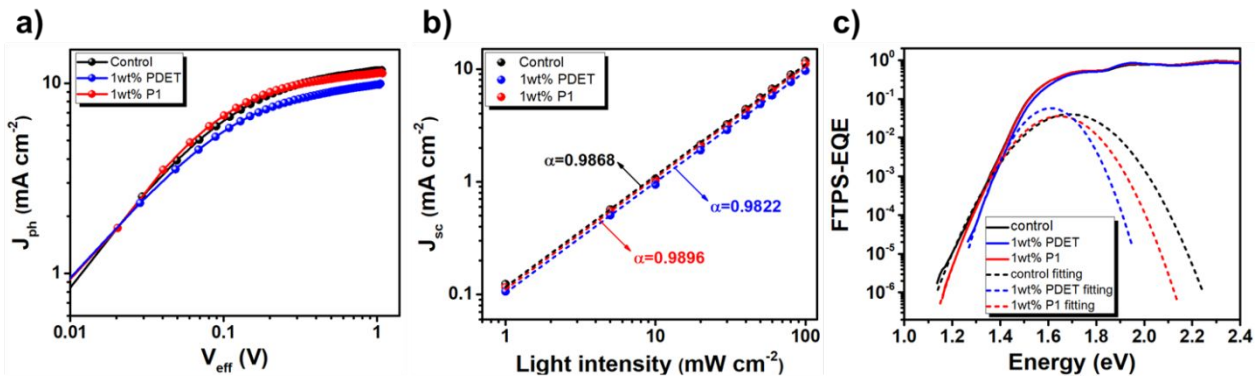

Figure 5. (a) J_{ph}-V_{eff} characteristics, (b) J_{SC}-light intensity fitting curves, and (c) normalized FTPS-EQE and the fitting curves of the fabricated all-PSCs using different compatibilizers.

To scrutinize the possible changes of the BHJ morphology, grazing incidence wide-angle X-ray diffraction scattering (GIWAXS) measurements of the control binary blend and the ternary blends with 1wt% **P1** and **PDET** prepared on the ZnO electron-transporting layer were carried out. Figure 6a-c represent their 2-D GIWAXS patterns and the detailed information of the peaks were depicted in Figure 6d. In the in-plane direction, all these films showed a similar (100) diffraction peak (q_{xy} = 0.159 Å^{-1}, 0.150 Å^{-1}, and 0.152 Å^{-1} for control, 1 wt% **P1**, and 1 wt% **PDET** films, respectively), corresponding to the lamellar stacking with a *d*-spacing of ~39-41 Å. The crystal coherence length (CCL) value was then calculated using the Scherrer equation of $2\pi/\Delta q$, where Δq represents the full width half maximum (FWHM) of diffraction peak obtained by Gaussian fitting. Both films with compatibilizers delivered a lower CCL value (107.96 Å for 1 wt% **P1** and 106.1 Å for 1 wt% **PDET**) than that (149.63 Å) of the control film. This result suggests that addition of **P1** and **PDET** suppresses the phase separation between the constituent components.[43]

For the diffraction in the out-of-plane direction, all of these films exhibited an obvious (010) peak at ~ 1.5 Å^{-1}, representing the face-on orientation of these polymer films. The control and 1 wt% **P1** films exhibited similar CCL values of 33.11 and 31.01 Å, respectively; whereas, the 1 wt% **PDET** film delivered a lowest CCL value of 27.24 Å. Moreover, an additional peak at q_z = 1 Å^{-1} with

different CCL values (20.45 Å, 17.46 Å, 17.42 Å for the control, 1 wt% **P1** and 1 wt% **PDET** films, respectively) were observed in these films. This peak can be attributed to the π-π stacking of PCE12.[62] These results thus indicate that the addition of **PDET** largely varies the polymer packing in the out-of-plane direction, which hampers the transport of charge carriers. Notably, another peak at $q_z = 0.19$ $Å^{-1}$ was found only for the control film but not for the other films. This suggests that the lamella packing of the polymers in the out-of-plane direction diminished after adding the compatibilizers, which enabled an easier formation of the face-on orientation for the BHJ films. In brief, the addition of **P1** suppresses the self-aggregation of photoactive components through facilitating their intermixing in the in-plane direction without impacting the π-π stacking in the out-of-plane direction, leading to better photovoltaic performances.

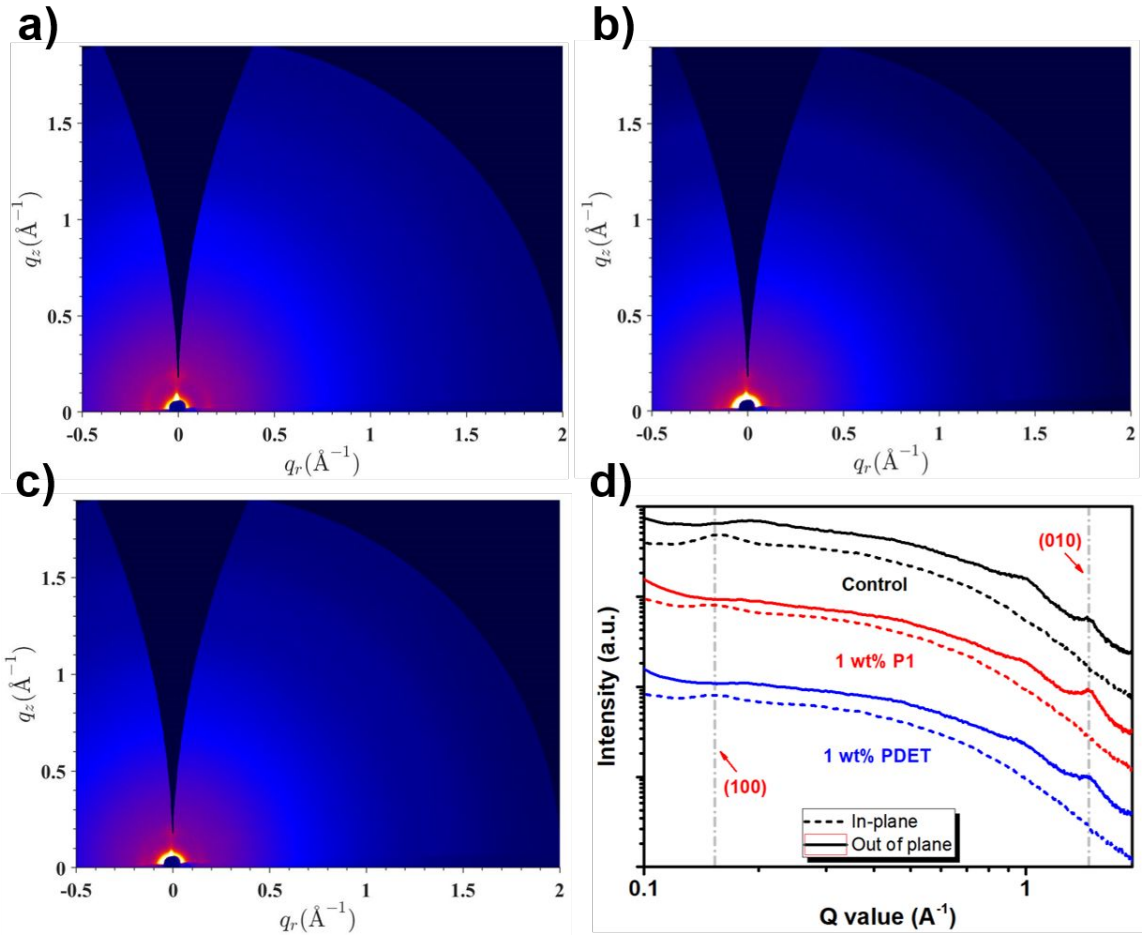

Figure 6. 2D GIWAXS patterns of (a) the binary PCE12:N2200 film and (b,c) the ternary blend films with different compatibilizers. (d) Their corresponding 1D linecuts in the out-of-plane (solid line) and in-plane (dotted line) directions.

We noticed that the V_{oc} was slightly improved for the 1 wt% **P1** device and it might have been associated with the reduction of potential loss. To clarify this, we measured the total energy loss (E_{loss}) for the control, 1 wt% **P1**, and 1wt% **PDET** devices using the Fourier transform photocurrent spectroscopy EQE (FTPS-EQE). Figure 5c presented the normalized curves along with the fitting curves of these devices and the relevant parameters are summarized in Table S2, ESI†. In principle, the total E_{loss} can be divided into three contributions: (i) charge generation (ΔE_2); (ii) radiative recombination (ΔE_1); (3) non-radiative recombination (ΔE_3), and it can be calculated by the following equation:[63,64]

$$E_{loss} = E_{gap} - qV_{oc}$$

$$= \left[-kT\ln\left(\frac{J_{sc}h^3c^2}{2\pi fq(E_{CT} - \lambda)}\right)\right] + (E_{gap} - E_{CT}) + [-kT\ln(EQE_{EL})]$$

$$= \Delta E_1 + \Delta E_2 + \Delta E_3$$

where k is the Boltzmann constant, T is the absolute temperature, h is the Planck's constant, q is the elementary charge, c is the speed of light, and EQE_{EL} is device's electroluminescence EQE.

As shown in Table S2, ESI†, the E_{CT} values for the control, 1 wt% **P1**, and 1 wt% **PDET** devices were 1.42, 1.44, and 1.46 eV, respectively, and all of them exhibited similar ΔE_1 values (0.26-0.27 eV) that are inherent to the devices. The ΔE_2 values for the control, 1 wt% **P1**, and 1 wt% **PDET** devices were 0.061, 0.047, and 0.056 eV, respectively. Note that the ΔE_2 values have been generally recognized to associate with the energetic offsets between the photoactive materials, and a smaller energetic offset results in a smaller ΔE_2 value.[65] The smallest ΔE_2 value observed for the 1 wt% **P1**

device clearly benefits from its compatibilizer effect that better optimizes the BHJ morphology of the photoactive blend. Adding additives increased the ΔE_3 value of the device, but compared to the 1wt% **PDET** device, the 1wt% **P1** device possessed a lower ΔE_3 value, indicating its superior capability to overcome the non-radiative recombination loss. Overall, the 1wt% **P1** device delivered the smallest E_{loss} among the studied devices, confirming the advantage of the block copolymer compatibilizer in reducing the potential loss.

Conclusions

Straightforward synthesis of triblock copolymers from **PDET** and PS-N_3 by using efficient Cu-catalyzed azide-alkyne click reaction was demonstrated in this study. The resulting triblock copolymers retained the optical and electrochemical properties of the starting **PDET**, which is advantageous for practical applications. Pure triblock copolymers exhibited signs of phase separation upon annealing to a temperature above the T_g of the PS block. One-step simple preparation of poly(arylenebutadiynylene)s and reliability of the azide-alkyne click reaction create a possibility of developing a variety of coil-rod-coil block copolymers. We finally explored the compatibilizer function of the starting **PEDT** and the derived triblock copolymers (**P1** as the representative) in an all-polymer solar cell based on the PCE12:N2200 blend. We found that adding 1 wt% **P1** can result in a relative ~6% enhancement in PCE, but adding 1 wt% **PDET** delivered a decreased performance. Besides elucidating **P1**'s compatibilizer function on tuning the BHJ morphology of the blend film, its effect on reducing device's potential loss was also investigated. Collectively, our results provide an efficient method of synthesizing versatile coil-rod-coil triblock copolymers and demonstrate their potential for photovoltaic applications.

Experimental

Materials and synthesis

All reagents and chemicals were purchased from Tokyo Chemical Industry (TCI), Kanto Chemical, Co., Inc., and Sigma-Aldrich and used as received unless otherwise stated. CuBr was purified by stirring in glacial acetic acid for 6 h, followed by filtering, washing with dry methanol and drying in a vacuum oven. Synthesis of DET monomer and **PDET$_{29}$** was reported before.[52] **PDET$_{38}$** and **PDET$_{55}$** were synthesized similar to **PDET$_{29}$**. PS_{37}-Br and PS_{64}-Br were synthesized by the modified literature procedure.[3,54] The polymerizations were carried out in an Ar-filled glovebox, and the initiator amount and reaction time were varied to achieve desired molecular weights and polydispersities. PS_{37}-N_3 and PS_{64}-N_3 were prepared as reported in literature.[54]

*Synthesis of **PDET$_{38}$** and **PDET$_{55}$**.*

Freshly column chromatographed solution of DET in *n*-hexane (ca. 500 mg mL^{-1}, 300 μL, 0.69 mmol) was added to a 4 mL chloroform solution of CuCl (1.8 mg mL^{-1}, 0.073 mmol) and TMEDA (22 μL mL^{-1}, 0.148 mmol). The reaction solution was stirred at room temperature for 40 min under slow bubbling with dry air. The solution was then concentrated by a rotary evaporator to ~2 mL and poured into methanol (60 mL) acidified with HCl (37%, 1 mL). The precipitate was collected by filtration, re-dissolved in chloroform (~2 mL), and precipitated into acetone (40 mL) to afford 88 mg of **PDET$_{38}$** (59% yield) as a reddish-brown solid. GPC (*o*-DCB): M_n = 8.14 kg mol^{-1}, PDI = 2.82. ^{1}H NMR ($CDCl_3$, ppm) δ: 7.09 (s), 3.49 (s) 2.67 (br), 1.60 (br), 1.31 (br), 0.90 (br). FTIR (cm^{-1}): 3309 (C≡C−H stretching), 2924, 2852 (C–H stretching), 2207, 2142 (C≡C−C≡C stretching), 2104 (C≡C stretching), 1728, 1645, 1598, 1518, 1465, 1437, 1393, 1376, 1299, 1264, 1242, 1170, 1111, 1078, 1023, 985, 954, 916, 876, 858, 837, 806, 721, 700, 657, 644, 631, 620.

The same procedure as above using the reaction time of 60 min afforded 105 mg of **PDET$_{55}$** (70% yield). GPC (*o*-DCB): M_n = 11.8 kg mol^{-1}, PDI = 2.83. ^{1}H NMR and FTIR spectra were identical to those of **PDET$_{38}$**.

Synthesis of PS_{37}-Br and PS_{64}-Br.

In an Ar-filled glovebox, CuBr (131 mg, 0.92 mmol), PMDETA (190 μL, 0.91 mmol) and methyl 2-bromopropionate (MBP, 100 μL, 0.92 mmol) were added to a mixture of styrene (10 mL, 91.6 mmol) and toluene (7 mL, 40% v/v) in a 30-mL sample tube. The tube was then quickly sealed and removed from the glovebox, placed into an oil bath and stirred at 80 °C for 4 h. The reaction was quenched by cooling to room temperature and exposing to air. After diluting with THF, the product mixture was passed through neutral alumina. The solution was concentrated and precipitated into methanol (150 mL) to afford 2.26 g of PS_{37}-Br as a white solid (24.8% yield). GPC (*o*-DCB, 40 °C): M_n = 3.97 kDa, PDI = 1.05. ^{1}H NMR ($CDCl_3$, ppm) δ: 6.27–7.26 (br, aromatic), 4.47 (br, CH−Br), 3.37–3.54 (s, OCH_3), 1.87–1.92 (br, CH_2), 1.48 (br, CH−Ph). FTIR (cm^{-1}): 3082, 3081, 3062, 3059, 3025, 3002, 3001, 2923, 2849 (C−H stretching), 2845, 1943, 1942, 1870, 1867, 1802, 1799, 1738, 1736, 1601, 1583, 1540, 1492, 1452 (C=C stretching), 1375, 1328, 1182, 1155, 1067, 907, 840, 754.

The same procedure as above afforded 3.04 g of PS_{64}-Br from 12 mL of styrene using the styrene/CuBr/PMDETA/MBP ratio of 200:1:1:1 (molar) and the reaction time of 9 h (27.8% yield). GPC (*o*-DCB, 40 °C): M_n = 6.85 kg mol^{-1}, PDI = 1.05. ^{1}H NMR and FTIR spectra were identical to those of PS_{37}-Br.

Synthesis of PS_{37}-N_3 and PS_{64}-N_3.

PS-Br was converted to the corresponding PS-N_3 by the reaction with NaN_3, as described in literature.[54] The reaction of 415 mg of PS_{37}-Br afforded 345 mg of PS_{37}-N_3 (83% yield). The yield was limited by the loss during filtration. Note that excess NaN_3 in the waste solution was deactivated with $NaNO_2$ in the presence of H_2SO_4. GPC (*o*-DCB, 40 °C): M_n = 4.01 kDa, PDI = 1.05. ^{1}H-NMR ($CDCl_3$, ppm) δ: 6.46–7.42 (br, aromatic), 3.90 (br, CH−N_3), 3.39–3.49 (m, OCH_3), 1.81–1.86 (br, CH_2), 1.44 (br, CH−Ph). FTIR (cm^{-1}): 3082, 3081, 3062, 3059, 3025, 3002, 3001, 2923, 2849 (C−H stretching), 2845, 2097 (N=N=N stretching), 1943, 1942, 1870, 1867, 1802, 1799, 1738, 1736, 1601,

1583, 1540, 1492, 1452 (C=C stretching), 1375, 1328, 1182, 1155, 1067, 1027, 907, 840, 754.

The same procedure as above afforded 1.90 g of PS_{64}-N_3 from 2.00 g of PS_{64}-Br (95% yield). GPC (*o*-DCB, 40 °C): M_n = 6.87 kg mol^{-1}, PDI = 1.05. ^{1}H-NMR and FTIR spectra were identical to those of PS_{37}-N_3.

*General procedure for the synthesis of **P1**, **P2**, **P3** and **P4**.*

A mixture of **PDET$_{29}$** (40 mg, 6.3 μmol, 1.0 eq.), PS_{37}-N_3 (63 mg, 15.9 μmol, 2.5 eq.), CuBr (8 mg, 55.8 mmol, 9 eq.) and PMDETA (21 μL, 100.6 μmol, 16 eq.) were dissolved in chlorobenzene (1 mL) in a 5-mL sample tube in an Ar-filled glovebox. In the glovebox, the solution was stirred on a hotplate at 80 °C for 4 h. The solution was cooled to room temperature and exposed to air. It was poured into methanol (40 mL) acidified with HCl (37%, 1 mL) to ensure the removal of the catalysts. The precipitate was collected by filtration and sonicated in acetone (30 mL) for 30 min to dissolve unreacted PS-N_3. The solid was collected by filtration. This process was repeated several times until the filtrate did not exhibit the characteristic N=N=N peak (2097 cm^{-1}) in the FTIR spectrum. Chloroform (20 mL) was added to the collected solid and the mixture was sonicated for 30 min. Undissolved solids were removed by filtration. The filtrate was concentrated and precipitated into methanol. The solid was collected by filtration and dried under vacuum to afford 41 mg of **P1** as a fluffy dark orange solid (45% yield). GPC (*o*-DCB): M_n = 13.6 kDa, PDI = 2.04. ^{1}H NMR ($CDCl_3$, ppm) δ: 6.46–7.42 (br), 7.09 (s), 3.39–3.49 (m), 2.67 (br), 1.81–1.86 (br), 1.60 (br), 1.44 (br, CH−Ph), 1.31 (br), 0.90 (br). FTIR (cm^{-1}): 3309 (C≡C−H stretching), 3082, 3081, 3062, 3059, 3025, 3002, 3001, 2923, 2849 (C−H stretching), 2207, 2142 (C≡C−C≡C stretching), 1943, 1942, 1870, 1867, 1802, 1799, 1738, 1736, 1728, 1645, 1601, 1598, 1583, 1540, 1518, 1492, 1465, 1452 (C=C stretching), 1437, 1393, 1376, 1328, 1299, 1264, 1242, 1182, 1170, 1155, 1111, 1078, 1067, 1027, 1023, 985, 954, 916, 907, 876, 858, 840, 837, 806, 754, 721, 700, 657, 644, 631, 620.

The same procedure as above afforded 40 mg of **P2** from **PDET$_{38}$** (38 mg, 4.7 μmol) and

PS_{37}-N_3 (48 mg, 12.0 μmol) in THF (1.3 mL) stirred at 60 °C for 7 h (53% yield). GPC (*o*-DCB): M_n = 16.2 kg mol^{-1}, PDI = 2.56. ^{1}H-NMR and FTIR spectra were identical to those of **P1**.

The same procedure as above afforded 30 mg of **P3** from **PDET$_{55}$** (40 mg, 3.40 μmol) and PS_{37}-N_3 (34 mg, 8.5 μmol) in THF (1.5 mL) stirred at 60 °C for 4 h (43% yield). GPC (*o*-DCB): M_n = 18.9 kg mol^{-1}, PDI = 2.34. ^{1}H-NMR and FTIR spectra were identical to those of **P1**.

The same procedure as above afforded 38 mg of **P4** from **PDET$_{55}$** (40 mg, 3.40 μmol) and PS_{64}-N_3 (58 mg, 8.5 μmol) in THF (1.5 mL) stirred at 60 °C for 4 h (42% yield). GPC (*o*-DCB): M_n = 23.5 kg mol^{-1}, PDI = 2.21. ^{1}H-NMR and FTIR spectra were identical to those of **P1**.

General measurements

^{1}H NMR (300 MHz) and ^{13}C NMR (75 MHz) were recorded on a JEOL AL-300 spectrometer using deuterated chloroform as the solvent. GPC was measured on a JASCO GULLIVER 1500 equipped with two Shodex GPC KF-803 columns (8.0 mm I.D. × 300 mm L) at 40 °C using *o*-dichlorobenzene (*o*-DCB) as the eluent with polystyrene standards. CV was measured on a BAS electrochemical analyzer model 612C in a three-electrode cell with the Ar-bubbled dehydrated acetonitrile solution of tetra-*n*-butylammonium hexafluorophosphate (0.1 M) at a sweep rate of 1 mV s^{-1}. The working, reference, and counter electrodes were glassy carbon, Ag/AgCl, and Pt wire, respectively. Polymer films were drop cast onto the working electrode from chloroform solutions. Redox potential of ferrocene/ferrocenium (Fc/Fc$^+$) was used for calibration. Attenuated total reflection FTIR spectroscopy was measured on a JASCO FT/IR 4200 spectrometer. TGA and DSC measurements were carried out using a Rigaku TG8120 and Rigaku DSC8230, respectively, under N_2 flow at the heating/cooling rate of 10 °C min^{-1}. UV-vis absorption spectra were recorded on a JASCO V-670 spectrophotometer. Tapping-mode AFM images was taken on a Seiko Instruments SPA-400 with a stiff cantilever Seiko Instruments DF-20. Grazing incidence wide-angle X-ray scattering (GIWAXS) data of the polymer films were carried out on beamlines 17A1 with a

wavelength of 1.321 Å in the National Synchrotron Radiation Research Center (NSRRC), Taiwan.

Device fabrication and characterization

An inverted device structure of ITO glass/ZnO/BHJ/MoO_3/Ag was fabricated in this work. The ITO glass substrates were sequentially washed by DI water, acetone, and isopropyl alcohol for 15 min each step. The dried ITO glass was then subjected to the plasma treatment for 10 min. The electron transporting ZnO layer was spin-coated on the ITO glass at 4000 rpm for 30 s and then dried at 180 ^{o}C for 30 min in air. The control precursor solution of PCE12:N2200 (2:1 weight ratio) with a concentration of 8 mg/mL was prepared in CB. Different compatibilizers with weight ratios of 1-3% were separately blended into the control precursor solution. All of the precursor solutions were vigorously stirred at 50 ^{o}C for 12 h in a N_2-filled glove box, followed by annealing at 100 ^{o}C for 10 min. The thickness of the BHJ layer was ~ 80-90 nm on the ZnO layer. Finally, 10 nm MoO_3 and 100 nm Ag were sequentially thermally deposited onto the BHJ layer to complete device fabrication. The active area for the device is 8.5 mm^2.

The current-voltage (*J-V*) characteristics of the devices were measured under AM 1.5G illumination (100 mW cm^{-2}) by a Newport LCS-100 simulator, which were recorded with a computer-controlled Keithley 2400 source measurement unit (SMU). The illumination intensity was calibrated by using a Si photodiode detector with a KG-5 filter. The external quantum efficiency (EQE) was measured by a monochromatic light from a xenon lamp during the illumination (QE-R, Enlitech Co., Ltd.) and using a standard single crystal Si photovoltaic cell to calibrate the light intensity under the wavelength from 300 to 900 nm. The FTPS-EQE was measured by the instrument of FTPS PECT-600 from Enlitech, which calculates the detailed parameter of energy loss.

Conflicts of interest

The authors declare no competing financial interest.

Acknowledgements

T. M. thanks financial supports from JSPS KAKENHI Grant 19H02786, JST ASTEP JPMJTM20CS, and the Heiwa Nakajima Foundation. C. C. C. gratefully thanks financial supports from Top University Project of National Taiwan University (110L7836) and the Featured Area Research Center Program within the framework of the Higher Education Sprout Project by the Ministry of Education (110L9006) and the Ministry of Science and Technology in Taiwan (MOST 110-2634-F-002-043, 109-2628-E-002-008-MY3, 110-2923-E-002-007-MY3, 110-2628-E-002-011-).

References

1. T. Higashihara, K. Sugiyama, H.-S. Yoo, M. Hayashi, A. Hirao, Combining Living Anionic Polymerization with Branching Reactions in an Iterative Fashion to Design Branched Polymers. *Macromol. Rapid Commun.*, 2010, **31**, 1031–1059.
2. G. Polymeropoulos, G. Zapsas, K. Ntetsikas, P. Bilalis, Y. Gnanou, N. Hadjichristidis, 50th Anniversary Perspective: Polymers with Complex Architectures. *Macromolecules*, 2017, **50**, 1253–1290.
3. A. P. Vogt, B. S. Sumerlin, An Efficient Route to Macromonomers via ATRP and Click Chemistry. *Macromolecules*, 2006, **39**, 5286–5292.
4. J. S. Kim, J. Han, Y. Kim, H. Park, J. P. Coote, G. E. Stein, B. J. Kim, Domain Structures of Poly(3-Dodecylthiophene)-Based Block Copolymers Depend on Regioregularity. *Macromolecules*, 2018, **51**, 4077–4084.
5. C. M. Loudy, J. Allouche, A. Bousquet, C. Courrèges, H. Martinez, L. Billon, Core@Corona Functional Nanoparticle-Driven Rod-Coil Diblock Copolymer Self-Assembly. *Langmuir*, 2019, **35**, 16925–16934.
6. H. Erothu, J. Kolomanska, P. Johnston, S. Schumann, D. Deribew, D. T. W. Toolan, A. Gregori, C. Dagron-Lartigau, G. Portale, W. Bras, T. Arnold, A. Distler, R. C. Hiorns, P. Mokarian-Tabari, T. W. Collins, J. R. Howse, P. D. Topham, Synthesis, Thermal Processing, and Thin Film

Morphology of Poly(3-hexylthiophene)-Poly(styrenesulfonate) Block Copolymers. *Macromolecules*, 2015, **48**, 2107–2117.

7. P. M. Reichstein, J. C. Brendel, M. Drechsler, M. Thelakkat, Poly(3-hexylthiophene)- *block*-Poly(tetrabutylammonium-4-styrenesulfonate) Block Copolymer Micelles for the Synthesis of Polymer Semiconductor Nanocomposites. *ACS Appl. Nano Mater.*, 2019, **2**, 2133–2143.
8. H. N. Choi, H. S. Yang, J. H. Chae, T. L. Choi, I. H. Lee, Synthesis of Conjugated Rod-Coil Block Copolymers by RuPhos Pd-Catalyzed Suzuki-Miyaura Catalyst-Transfer Polycondensation: Initiation from Coil-Type Polymers. *Macromolecules*, 2020, **53**, 5497–5503.
9. W. Wang, T. Li, T. Yu, F. Zhu, Synthesis of Multiblock Copolymers by Coupling Reaction Based on Self-Assembly and Click Chemistry Synthesis of Multiblock Copolymers by Coupling Reaction Based on Self-Assembly and Click Chemistry. *Macromolecules*, 2008, **41**, 9750–9754.
10. X. He, L. Liang, M. Xie, Y. Zhang, S. Lin, D. Yan, Synthesis of Novel Linear PEO-*b*-PS-*b*-PCL Triblock Copolymers by the Combination of ATRP, ROP, and a Click Reaction. *Macromol. Chem. Phys.*, 2007, **208**, 1797–1802.
11. S. Reinicke, H. Schmalz, Combination of Living Anionic Polymerization and ATRP via "Click" Chemistry as a Versatile Route to Multiple Responsive Triblock Terpolymers and Corresponding Hydrogels. *Colloid Polym. Sci.*, 2011, **289**, 497–512.
12. K. Wang, L. Liang, S. Lin, X. He, Synthesis of Well-Defined ABC Triblock Copolymers with Polypeptide Segments by ATRP and Click Reactions. *Eur. Polym. J.*, 2008, **44**, 3370–3376.
13. H. Sun, I. H. Öner, T. Wang, T. Zhang, O. Selyshchev, C. Neumann, Y. Fu, Z. Liao, S. Xu, Y. Hou, A. Turchanin, D. R. T. Zahn, E. Zschech, I. M. Weidinger, J. Zhang, X. Feng, Molecular Engineering of Conjugated Acetylenic Polymers for Efficient Cocatalyst-free Photoelectrochemical Water Reduction. *Angew. Chem. Int. Ed.*, 2019, **58**, 10368–10374.
14. S. Otep, T. Michinobu, Q. Zhang, Pure Organic Semiconductor-Based Photoelectrodes for Water Splitting. *Sol. RRL*, 2020, **4**, 1900395.
15. J. Zhao, Y. Li, G. Yang, K. Jiang, H. Lin, H. Ade, W. Ma, H. Yan, Efficient Organic Solar Cells Processed from Hydrocarbon Solvents. *Nat. Energy*, 2016, **1**, 15027.
16. D. Deng, Y. Zhang, J. Zhang, Z. Wang, L. Zhu, J. Fang, B. Xia, Z. Wang, K. Lu, W. Ma, Z. Wei, Fluorination-Enabled Optimal Morphology Leads to over 11% Efficiency for Inverted Small-Molecule Organic Solar Cells. *Nat. Commun.*, 2016, **7**, 13740.
17. G. Zhang, K. Zhang, Q. Yin, X. F. Jiang, Z. Wang, J. Xin, W. Ma, H. Yan, F. Huang, Y. Cao, High-Performance Ternary Organic Solar Cell Enabled by a Thick Active Layer Containing a Liquid Crystalline Small Molecule Donor. *J. Am. Chem. Soc.*, 2017, **139**, 2387–2395.

18. Y. Lin, Y. Firdaus, M. I. Nugraha, F. Liu, S. Karuthedath, A. H. Emwas, W. Zhang, A. Seitkhan, M. Neophytou, H. Faber, E. Yengel, I. McCulloch, L. Tsetseris, F. Laquai, T. D. Anthopoulos, 17.1% Efficient Single-Junction Organic Solar Cells Enabled by n-Type Doping of the Bulk-Heterojunction. *Adv. Sci.*, 2020, **7**, 1903419.
19. Y. Cui, H. Yao, L. Hong, T. Zhang, Y. Tang, B. Lin, K. Xian, B. Gao, C. An, P. Bi, J. Hou, Organic Photovoltaic Cell with 17% Efficiency and Superior Processability. *Natl. Sci. Rev.*, 2020, **7**, 1239–1246.
20. Q. Liu, Y. Jiang, K. Jin, J. Qin, J. Xu, W. Li, J. Xiong, J. Liu, Z. Xiao, K. Sun, S. Yang, X. Zhang, L. Ding, 18% Efficiency Organic Solar Cells. *Sci. Bull.*, 2020, **65**, 272–275.
21. B. Fan, L. Ying, P. Zhu, F. Pan, F. Liu, J. Chen, F. Huang, Y. Cao, All-Polymer Solar Cells Based on a Conjugated Polymer Containing Siloxane-Functionalized Side Chains with Efficiency over 10%. *Adv. Mater.*, 2017, **29**, 1703906.
22. B. Fan, L. Ying, Z. Wang, B. He, X. F. Jiang, F. Huang, Y. Cao, Optimisation of Processing Solvent and Molecular Weight for the Production of Green-Solvent-Processed All-Polymer Solar Cells with a Power Conversion Efficiency over 9%. *Energy Environ. Sci.*, 2017, **10**, 1243–1251.
23. J. Yang, B. Xiao, S. W. Heo, K. Tajima, F. Chen, E. Zhou, Effects of Inserting Thiophene as a □-Bridge on the Properties of Naphthalene Diimide-alt-Fused Thiophene Copolymers. *ACS Appl. Mater. Interfaces*, 2017, **9**, 44070–44078.
24. N. B. Kolhe, H. Lee, D. Kuzuhara, N. Yoshimoto, T. Koganezawa, S. A. Jenekhe, All-Polymer Solar Cells with 9.4% Efficiency from Naphthalene Diimide-Biselenophene Copolymer Acceptor. *Chem. Mater.*, 2018, **30**, 6540–6548.
25. N. Zhou, A. Facchetti, Naphthalenediimide (NDI) Polymers for All-Polymer Photovoltaics. *Mater. Today*, 2018, **21**, 377–390.
26. X. Liu, Y. Zou, H. Q. Wang, L. Wang, J. Fang, C. Yang, High-Performance All-Polymer Solar Cells with a High Fill Factor and a Broad Tolerance to the Donor/Acceptor Ratio. *ACS Appl. Mater. Interfaces*, 2018, **10**, 38302–38309.
27. A. Robitaille, S. A. Jenekhe, M. Leclerc, Poly(naphthalene diimide-*alt*-bithiophene) Prepared by Direct (Hetero)Arylation Polymerization for Efficient All-Polymer Solar Cells. *Chem. Mater.*, 2018, **30**, 5353–5361.
28. J. Yuan, Y. Xu, G. Shi, X. Ling, L. Ying, F. Huang, T. H. Lee, H. Y. Woo, J. Y. Kim, Y. Cao, W. Ma, Engineering the Morphology *via* Processing Additives in Multiple All-Polymer Solar Cells for Improved Performance. *J. Mater. Chem. A*, 2018, **6**, 10421–10432.
29. G. Wang, F. S. Melkonyan, A. Facchetti, T. J. Marks, All-Polymer Solar Cells: Recent Progress,

Challenges, and Prospects. *Angew. Chem. Int. Ed.*, 2019, **58**, 4129–4142.

30. C. Lee, S. Lee, G.-U. Kim, W. Lee, B. J. Kim, Recent Advances, Design Guidelines, and Prospects of All-Polymer Solar Cells. *Chem. Rev.*, 2019, **119**, 8028–8086.
31. Z. Li, L. Ying, P. Zhu, W. Zhong, N. Li, F. Liu, F. Huang, Y. Cao, A Generic Green Solvent Concept Boosting the Power Conversion Efficiency of All-Polymer Solar Cells to 11%. *Energy Environ. Sci.*, 2019, **12**, 157–163.
32. H. Yao, F. Bai, H. Hu, L. Arunagiri, J. Zhang, Y. Chen, H. Yu, S. Chen, T. Liu, J. Y. L. Lai, Y. Zou, H. Ade, H. Yan, Efficient All-Polymer Solar Cells Based on a New Polymer Acceptor Achieving 10.3% Power Conversion Efficiency. *ACS Energy Lett.*, 2019, **4**, 417–422.
33. Y. Wang, S. W. Kim, J. Lee, H. Matsumoto, B. J. Kim, T. Michinobu, Dual Imide-Functionalized Unit-Based Regioregular D-A_1-D-A_2 Polymers for Efficient Unipolar n-Channel Organic Transistors and All-Polymer Solar Cells. *ACS Appl. Mater. Interfaces*, 2019, **11**, 22583–22594.
34. S. W. Kim, Y. Wang, H. You, W. Lee, T. Michinobu, B. J. Kim, Impact of Incorporating Nitrogen Atoms in Naphthalenediimide-Based Polymer Acceptors on the Charge Generation, Device Performance, and Stability of All-Polymer Solar Cells. *ACS Appl. Mater. Interfaces*, 2019, **11**, 35896–35903.
35. A. Bonasera, G. Giuliano, G. Arrabito, B. Pignataro, Tackling Performance Challenges in Organic Photovoltaics: An Overview about Compatibilizers. *Molecules*, 2020, **25**, 1–39.
36. M. Saito, Y. Tamai, H. Ichikawa, H. Yoshida, D. Yokoyama, H. Ohkita, I. Osaka, Significantly Sensitized Ternary Blend Polymer Solar Cells with a Very Small Content of the Narrow-Band Gap Third Component That Utilizes Optical Interference. *Macromolecules*, 2020, **53**, 10623–10635.
37. N. Gasparini, A. Salleo, I. McCulloch, D. Baran, The Role of the Third Component in Ternary Organic Solar Cells. *Nat. Rev. Mater.*, 2019, **4**, 229–242.
38. L. Ye, X. Jiao, W. Zhao, S. Zhang, H. Yao, S. Li, H. Ade, J. Hou, Manipulation of Domain Purity and Orientational Ordering in High Performance All-Polymer Solar Cells. *Chem. Mater.*, 2016, **28**, 6178–6185.
39. H. I. Kim, M. Kim, C. W. Park, H. U. Kim, H. K. Lee, T. Park, Morphological Control of Donor/Acceptor Interfaces in All-Polymer Solar Cells Using a Pentafluorobenzene-Based Additive. *Chem. Mater.*, 2017, **29**, 6793–6798.
40. S. Liu, D. Chen, W. Zhou, Z. Yu, L. Chen, F. Liu, Y. Chen, Vertical Distribution to Optimize Active Layer Morphology for Efficient All-Polymer Solar Cells by J71 as a Compatibilizer. *Macromolecules*, 2019, **52**, 4359–4369.

41. H. Fujita, T. Michinobu, M. Tokita, M. Ueda, T. Higashihara, Synthesis and Postfunctionalization of Rod-Coil Diblock and Coil-Rod-Coil Triblock Copolymers Composed of Poly(3-hexylthiophene) and Poly(4-(4'-*N*,*N*-dihexylaminophenylethynyl)styrene) Segments. *Macromolecules*, 2012, **45**, 9643–9656.
42. H. Fujita, T. Michinobu, S. Fukuda, T. Koganezawa, T. Higashihara, Sequentially Different AB Diblock and ABA Triblock Copolymers as P3HT:PCBM Interfacial Compatibilizers for BHJ Photovoltaics. *ACS Appl. Mater. Interfaces*, 2016, **8**, 5484–5492.
43. Y.-A. Su, N. Maebayashi, H. Fujita, Y.-C. Lin, C.-I. Chen, W.-C. Chen, T. Michinobu, C.-C. Chueh, T. Higashihara, Development of Block Copolymers with Poly(3-hexylthiophene) Segments as Compatibilizers in Non-Fullerene Organic Solar Cells. *ACS Appl. Mater. Interfaces*, 2020, **12**, 12083–12092.
44. J. Chen, X. Yu, K. Hong, J. M. Messman, D. L. Pickel, K. Xiao, M. D. Dadmun, J. W. Mays, A. J. Rondinone, B. G. Sumpter, S. M. Kilbey, II. Ternary Behavior and Systematic Nanoscale Manipulation of Domain Structures in P3HT/PCBM/P3HT-*b*-PEO Films. *J. Mater. Chem.*, 2012, **22**, 13013–13022.
45. D. Kipp, V. Ganesan, Exploiting the Combined Influence of Morphology and Energy Cascades in Ternary Blend Organic Solar Cells Based on Block Copolymer Additives. *Macromolecules*, 2016, **49**, 5137–5144.
46. D. Kipp, R. Verduzco, V. Ganesan, Block Copolymer Compatibilizers for Ternary Blend Polymer Bulk Heterojunction Solar Cells – An Opportunity for Computation Aided Molecular Design. *Mol. Syst. Des. Eng.*, 2016, **1**, 353–369.
47. Y. Sun, P. Pitliya, C. Liu, X. Gong, D. Raghavan, A. Karim, Block Copolymer Compatibilized Polymer:Fullerene Blend Morphology and Properties. *Polymer*, 2017, **113**, 135–146.
48. E. Mohammadi-Arbati, S. Agbolaghi, Efficiency above 6% in Poly(3-Hexylthiophene):Phenyl-C-Butyric Acid Methyl Ester Photovoltaics via Simultaneous Addition of Poly(3-Hexylthiophene) Based Grafted Graphene Nanosheets and Hydrophobic Block Copolymers. *Polym. Int.*, 2019, **68**, 1292–1302.
49. H. J. Kim, J. H. Kim, J. H. Ryu, Y. Kim, H. Kang, W. B. Lee, T. S. Kim, B. J. Kim, Architectural Engineering of Rod-Coil Compatibilizers for Producing Mechanically and Thermally Stable Polymer Solar Cells. *ACS Nano*, 2014, **8**, 10461–10470.
50. M. Zhu, H. Kim, Y. J. Jang, S. Park, D. Y. Ryu, K. Kim, P. Tang, F. Qiu, D. H. Kim, J. Peng, Toward High Efficiency Organic Photovoltaic Devices with Enhanced Thermal Stability

Utilizing P3HT-*b*-P3PHT Block Copolymer Additives. *J. Mater. Chem. A*, 2016, **4**, 18432–18443.

51. A. Kato, L.-Y. Su, Y.-C. Lin, L. Wang, W.-C. Chen, C.-C. Chueh, T. Higashihara, Naphthalene-diimide-based All-conjugated Block Copolymer as an Effective Compatibilizer to Improve the Performance and Thermal Stability of All-polymer Solar Cells. *Mater. Chem. Front.*, 2021, **5**, 7216–7227.
52. S. Otep, K. Ogita, N. Yomogita, K. Motai, Y. Wang, Y.-C. Tseng, C.-C. Chueh, Y. Hayamizu, H. Matsumoto, K. Ishikawa, T. Mori, T. Michinobu, Cross-linking of Poly(arylenebutadiynylene)s and Its Effect on Charge Carrier Mobilities in Thin Film Transistors. *Macromolecules*, 2021, **54**, 4351–4362.
53. J. F. Lutz, K. Matyjaszewski, Nuclear Magnetic Resonance Monitoring of Chain-End Functionality in the Atom Transfer Radical Polymerization of Styrene. *J. Polym. Sci. Part A: Polym. Chem.*, 2005, **43**, 897–910.
54. K. Ishizuki, H. Oka, D. Aoki, R. Goseki, H. Otsuka, Mechanochromic Polymers That Turn Green Upon the Dissociation of Diarylbibenzothiophenonyl: The Missing Piece toward Rainbow Mechanochromism. *Chem. Eur. J.*, 2018, **24**, 3170–3173.
55. D. R. Rutherford, J. K. Stille, C. M. Elliott, V. R. Reichert, Poly(2,5-Ethynylenethiophenediylethynylenes), Related Heteroaromatic Analogues, and Poly(Thieno[3,2-*b*]Thiophenes). Synthesis and Thermal and Electrical Properties. *Macromolecules*, 1992, **25**, 2294–2306.
56. G. L'abbe, Decomposition and Addition Reactions of Organic Azides. *Chem. Rev.*, 1969, **69**, 345–363.
57. H. Bassler, K. Anna, Charge Transport in Organic Semiconductors. In *Unimolecular and Supramolecular Electronics I*; Metzger, R. M., Ed.; Springer: Berlin, Heidelberg, 2011.
58. F. C. Spano, C. Silva, H- and J-Aggregate Behavior in Polymeric Semiconductors. *Annu. Rev. Phys. Chem.*, 2014, **65**, 477–500.
59. L. Lu, T. Xu, W. Chen, E. S. Landry, L. Yu, Ternary Blend Polymer Solar Cells with Enhanced Power Conversion Effeiciency. *Nat. Photon.*, 2014, **8**, 716–722.
60. P. Yin, T. Zheng, Y. Wu, G. Liu, Z.-G. Zhang, Z. Cui, Y. Li, P. Shen, Achieving Efficient Thick Active Layer and Large Area Ternary Polymer Solar Cells by Incorporating a New Fused Heptacyclic Non-fullerene Acceptor. *J. Mater. Chem. A*, 2018, **6**, 20313–20326.
61. A. Yin, D. Zhang, S.-H. Cheung, S.-K. So, Z. Fu, L. Ying, F. Huang, H. Zhou, Y. Zhang, On the Understanding of Energetic Disorder, Charge Recombination and Voltage Loss in All-Polymer

Solar Cells. *J. Mater. Chem. C*, 2018, **6**, 7855–7863.

62. Y. Zhang, Y. Xu, M. J. Ford, F. Li, J. Sun, X. Ling, Y. Wang, J. Gu, J. Yuan, W. Ma, Thermally Stable All-Polymer Solar Cells with High Tolerance on Blend Ratios. *Adv. Energy Mater.*, 2018, **8**, 1800029.
63. J. Zhang, W. Liu, M. Zhang, Y. Liu, G. Zhou, S. Xu, F. Zhang, H. Zhu, F. Liu, X. Zhu, Revealing the Critical Role of HOMO Alignment on Maximizing Current Extraction and Suppressing Energy Loss in Organic Solar Cells. *iScience*, 2019, **19**, 883–893.
64. Z. Zhou, S. Xu, J. Song, Y. Jin, Q. Yue, Y. Qian, F. Liu, F. Zhang, X. Zhu, High-efficiency Small-molecule Ternary Solar Cells with a Hierarchical Morphology Enabled by Synergizing Fullerene and Non-fullerene Acceptors. *Nat. Energy*, 2018, **3**, 952–959.
65. S. M. Menke, N. A. Ran, G. C. Bazan, R. H. Friend, Understanding Energy Loss in Organic Solar Cells: Toward a New Efficiency Regime. *Joule*, 2018, **2**, 25–35.